



HAL
open science

Accurate Prediction of the S 1 Excitation Energy in Solvated Azobenzene Derivatives via Embedded Orbital-Tuned Bethe-Salpeter Calculations

Aseem Rajan Kshirsagar, Gabriele D'avino, Xavier Blase, Jing Li, Roberta Poloni

► **To cite this version:**

Aseem Rajan Kshirsagar, Gabriele D'avino, Xavier Blase, Jing Li, Roberta Poloni. Accurate Prediction of the S 1 Excitation Energy in Solvated Azobenzene Derivatives via Embedded Orbital-Tuned Bethe-Salpeter Calculations. *Journal of Chemical Theory and Computation*, 2020, 16 (4), pp.2021-2027. 10.1021/acs.jctc.9b01257 . hal-02503936

HAL Id: hal-02503936

<https://hal.science/hal-02503936v1>

Submitted on 8 Dec 2020

HAL is a multi-disciplinary open access archive for the deposit and dissemination of scientific research documents, whether they are published or not. The documents may come from teaching and research institutions in France or abroad, or from public or private research centers.

L'archive ouverte pluridisciplinaire **HAL**, est destinée au dépôt et à la diffusion de documents scientifiques de niveau recherche, publiés ou non, émanant des établissements d'enseignement et de recherche français ou étrangers, des laboratoires publics ou privés.

Accurate prediction of the S_1 excitation energy in solvated azobenzene derivatives via embedded orbital-tuned Bethe-Salpeter calculations

Aseem Rajan Kshirsagar,[†] Gabriele D’Avino,[‡] Xavier Blase,[‡] Jing Li,^{*,‡,¶} and Roberta Poloni^{*,†}

[†]Grenoble-INP, SIMaP, University of Grenoble-Alpes, CNRS, F-38042 Grenoble, France

[‡]Institut Néel-CNRS and Université Grenoble-Alpes, F-38042 Grenoble, France

[¶]Université Grenoble-Alpes, CEA, IRIG, MEM-L_Sim, F-38000 Grenoble, France

Received March 5, 2020; E-mail: jing.li@cea.fr; roberta.poloni@grenoble-inp.fr

Abstract: By employing the Bethe-Salpeter formalism coupled with a non-equilibrium embedding scheme, we demonstrate that the paradigmatic case of S_1 band separation between *cis* and *trans* in azobenzene derivatives can be computed with excellent accuracy compared to experimental optical spectra. Besides embedding, we show that the choice of the Kohn-Sham exchange correlation functional for DFT is critical, despite the iterative convergence of GW quasiparticle energies. We address this by adopting an orbital-tuning approach via the global hybrid functional, PBEh, yielding an environment-consistent ionization potential. The vertical excitation energy of 20 azo molecules are predicted with a mean absolute error as low as 0.06 eV, up to three times smaller compared to standard functionals such as M06-2X and PBE0, and five times smaller compared to recent TDDFT results.

In recent years, molecular photoswitches have attracted much attention from researchers in different disciplines since they offer an efficient way to achieve light-harvesting through molecular functionalization. Azobenzene (**AB**) and its derivatives constitute an important family of molecular photoswitches which has found a variety of applications such as in drug delivery,^{1,2} DNA and RNA manipulation,^{3,4} gas separation using metal-organic framework scaffolds,⁵⁻⁷ and many more.

The *trans-cis* isomerization in **AB** occurs upon UV or visible light irradiation. For device design, the yield of isomerization should be as high as possible to achieve the largest possible change in the physical properties of the system.^{5,6} An efficient way to achieve high fractions of *cis* or *trans* is to irradiate using wavelengths that give a selective absorption of one isomer over the other.^{8,9} In the case of **AB**, only an incomplete yield of isomerization can be obtained upon $n \rightarrow \pi^*$ (S_1) excitation because of the S_1 optical bands of *cis* and *trans* largely overlap.¹⁰ In this regard, azobenzene functionalization has been proposed as a successful way to separate the S_1 between *trans* and *cis* and thus achieve almost complete fractions of each isomer at the photostationary state.^{11,12}

In order to assist experimental efforts devoted to material design using azobenzene derivatives, and other photoactive molecules in general, computational methods yielding an accuracy of below a tenth of eV are required. In this Letter, we demonstrate that the Bethe-Salpeter equation (BSE)/ GW formalism coupled with a non-equilibrium embedding scheme can yield excitation energies of the S_1 in azobenzene derivatives in excellent agreement with experiments, yielding a mean absolute error as low as 0.06 eV which is up to five times smaller compared to recent time-

dependent density functional theory (TDDFT) calculations performed with embedding.¹³ Our approach is based on two main points. The first is that environment effects are taken into account both at the ground state level and the BSE/ GW level by computing, respectively, the solvent-polarized Kohn-Sham (KS) ground state and the reaction field describing the *fast* electronic response of the environment to excitations, employing here a discrete polarizable model. The second aspect addresses the large dependence found here of the computed optical spectra on the starting point functional. The DFT starting point is here chosen in accordance to the ionization potential theorem for KS DFT (i.e. $\epsilon_H = -IP$, with $IP =$ ionization potential)¹⁴⁻¹⁸ thus yielding a different starting point functional in gas phase than in solution.

The BSE/ GW formalism,¹⁹ which was originally developed and then applied in the condensed matter community to describe optical excitations in semiconductors,¹⁹⁻²¹ has recently attracted attention even in the world of molecular systems,²²⁻²⁴ due to its accuracy and efficiency compared with wavefunction-based methods like CASPT2^{25,26} or coupled-cluster,²⁷ and its ability to overcome some of the limitations of TDDFT such as charge-transfer excitations and Rydberg excitations.^{22,28} Additionally, compared to TDDFT, the BSE/ GW approach has two advantages, i) higher accuracy of GW quasiparticle eigenvalues as compared to KS eigenvalues and ii) accurate asymptotic behavior of the two-particle (electron and hole) BSE Hamiltonian.²⁹ It is a two-step approach. First, within the GW many-body perturbation theory, where G is the time-ordered single-particle Green’s function and W the screened Coulomb potential, the KS eigenvalues are corrected perturbatively yielding the *true* energies to add or remove one electron, also referred to as quasiparticle (QP) energies. The second step is to use BSE to describe a two-particle bound state, i.e. the excited electron and the hole that it leaves behind. Recently, the BSE/ GW formalism has been further developed to incorporate the effects of classically described environments.³⁰⁻³³

In this work, we use the BSE/ GW as implemented in the FIESTA package,^{34,35} starting from the KS states (ϵ_n^{KS} , ϕ_n^{KS}) obtained from a DFT calculation using the NWCHEM package.³⁶ We perform eigenvalue self-consistent $evGW$ calculations updating that the GW quasiparticle energy of n level is updated iteratively without updating the KS wavefunction.^{35,37} Hence, the quasiparticle energy reads:

$$\epsilon_n^{GW} = \epsilon_n^{KS} + \langle \phi_n^{KS} | \Sigma^{GW}(\epsilon_n^{GW}) - V^{XC} | \phi_n^{KS} \rangle, \quad (1)$$

and it converges normally within a few iterations.

To compute accurately the optical spectra of solvated molecules, the solvation effects need to be taken into account since they are known to bring significant changes in

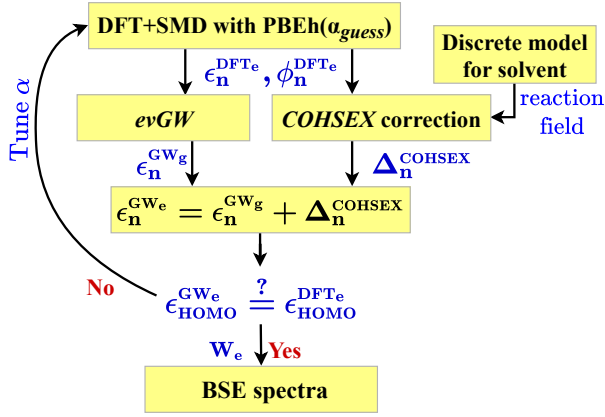


Figure 1. Workflow of the non-equilibrium embedded BSE/*GW* scheme adopted in this work.

the spectral features, as discussed for the case of azobenzene in the review work by Bandara and Burdette.¹⁰ Here, we employ a QM/MM (Quantum Mechanics/Molecular Mechanics) approach where the solvent is accounted for at both the DFT and BSE/*GW* level. To describe the ground state polarization effects, among available polarizable continuum models (PCM), we employ the solvation model based on the density (SMD)³⁸ whose parameters are taken from the Minnesota solvent descriptor database.³⁹ At BSE/*GW* level, the *fast* electronic response of the MM part is described by the reaction field matrix calculated using the solvent optical dielectric constant, ϵ_{opt} , which adds the contribution of the reaction field from the MM part to the screened Coulomb potential, W ^{31,32,40,41}. Specifically, starting from the screened Coulomb potential, W , verifying the Dyson equation for the gas-phase molecule:

$$W(r, r'; \omega) = v(r, r') + \int dr_1 dr_2 v(r, r_1) \chi_0(r_1, r_2; \omega) W(r_2, r'; \omega) \quad (2)$$

with χ_0 being the independent-particle susceptibility, the solvent effects are incorporated by solving the following set of equations, written in compact notation:

$$\tilde{v} = v + v\chi^{MM}v \quad (3)$$

$$W_e = \tilde{v} + \tilde{v}\chi_0 W_e \quad (4)$$

where the screened Coulomb potential incorporating solvent effects is W_e and the modified Coulomb potential, \tilde{v} , is the bare Coulomb potential, v , plus a renormalization term including the solvent reaction field. To avoid dealing with a full frequency-dependent χ^{MM} , we follow Refs.^{40,41} and adopt a strategy that consists in merging the low-frequency optical limit of *GW* with a discrete polarizable model that uses a low-frequency optical dielectric constant (e.g. $\epsilon_{opt}=1.77$ for methanol). The static Coulomb-hole plus screened exchange (COHSEX) approach is thus used to calculate W_e and the difference between COHSEX self-energy calculated with and without solvent is added to the *evGW* eigenvalues to get the $\epsilon_n^{GW_e}$:

$$\begin{aligned} \epsilon_n^{GW_e} &\approx \epsilon_n^{GW} + \Delta\epsilon_n^{COHSEX} \\ &= \epsilon_n^{GW} + \langle \phi_n^{KS} | \Sigma^{COHSEX/MM} - \Sigma^{COHSEX} | \phi_n^{KS} \rangle \end{aligned} \quad (5)$$

The W_e is subsequently used for building the BSE hamiltonian. Fig. 1 illustrates the whole computational scheme.

This embedded many-body perturbation approach includes the environmental dielectric effect on both

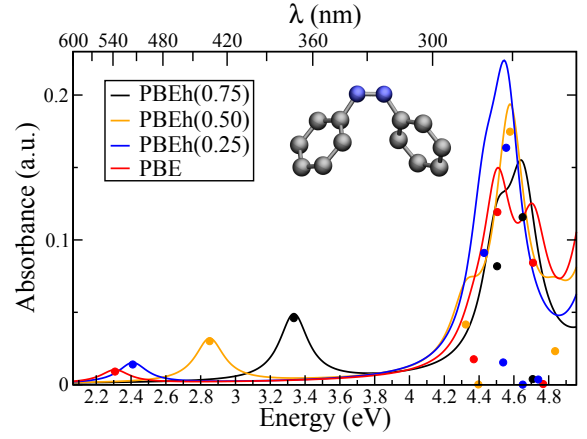


Figure 2. Optical spectra of *cis*-**AB** in gas phase calculated with BSE/*GW*/DFT@PBEh(α), with α being the fraction of exact exchange. The spectra show a large dependence on DFT functional. $E(S_1)$ increases by around 1 eV when α is increased from 0 to 0.75.

charged^{31,40} and neutral excitations,⁴¹ and has demonstrated the accuracy of the order of a tenth of eV in the prediction of the ionization potential.³² Both *linear response* and *state specific* solvent contributions are accounted for in the present BSE scheme.⁴¹ In this work, the reaction field matrix is determined by a discrete polarizable model using the MESCAL code.⁴² The solvent is described by a cubic lattice of polarizable points with the polarizability determined by the Clausius-Mossotti relation. The convergence studies for the solvent model is reported in SI (Table S2 and S3) together with validation against literature data computed using the more standard PCM approach (Table S4). The optical dielectric constant, ϵ_{opt} , is computed from the index of refraction at optical frequencies tabulated in the Minnesota solvent descriptor database.⁴³ To distinguish the embedded calculations from the gas phase, we use the symbol GW_e in contrast to GW_g and similar symbols are used for DFT calculations. DFT_e refers to DFT with SMD. We name the full embedding scheme BSE/ GW_e /DFT_e. The spectra are shown by multiplying the oscillator strength by a Lorentzian of 0.1 eV broadening (HWHM). Geometrical optimization of **AB** and its derivatives is computed with NWChem by employing cc-pVTZ/PBE0/SMD level^{38,44,45} while the aug-cc-pVDZ basis set⁴⁶ is employed for the rest of the DFT calculations needed to generate the KS eigenstates for subsequent *GW* and BSE calculations.

Because we employ the *evGW* approach, a dependence on the DFT starting point one-body wavefunctions may be expected. Therefore, the choice of the exchange and correlation functional (XCF) may become important. To illustrate this, we compare the BSE spectra of **AB** computed with different DFT starting points (see Fig. 2), using a hybrid functional,^{44,47} PBEh(α), by varying the amount of exact exchange α . PBEh⁴⁴ XCF is expressed as:

$$E_{XC}^{PBEh} = \alpha E_X^{exact} + (1 - \alpha) E_X^{PBE} + E_C^{PBE}, \alpha \in [0, 1]. \quad (6)$$

where E_X^{exact} is the exact exchange, E_X^{PBE} and E_C^{PBE} are PBE exchange and correlation,⁴⁸ respectively. Fig. 2 demonstrates a notable change on both the excitation energy and the oscillator strength as a function of the XCF. Specifically, the first excitation energy of *cis*-**AB**, $E(S_1)$, changes by as much as ~ 1 eV from α equal to 0 (i.e. PBE) to 0.75, while the oscillator strength changes from 0.009 to 0.044. In agreement with previous works,^{22,49} we observe a larger

dependence of S_1 , exhibiting a $n \rightarrow \pi^*$ character, than S_2 (with $\pi \rightarrow \pi^*$ character) on the XCF choice. A similar dependence is found for **AB-trans** (see Fig. S1). Such a large discrepancy on optical spectra can be attributed to significant changes in the input KS wavefunctions from one functional to another (see Fig. S3 and S4). The same qualitative result is obtained when comparing different functionals within the M06 series⁵⁰ (see Fig. S2 in SI).

To avoid such impasse, we choose a starting XCF that fulfills the ionization potential theorem.^{14–18} Practically, we choose a value of α that minimizes the following quantity,

$$J(\alpha) = \left| \epsilon_H^{evGW}(\alpha) - \epsilon_H^{KS}(\alpha) \right|, \quad (7)$$

which is the difference between the HOMO energies in $evGW$ and DFT. The IP is approximated here by the quasiparticle energy, $evGW$, computed at each value of α . This approach allows us to resolve the arbitrariness in the choice of the starting XCF while improving the asymptotic decay of the density. Because the highest occupied KS orbital dominates the asymptotic decay of the density^{51–53} ($\phi_H^{KS}(r) \rightarrow e^{-\sqrt{-2\epsilon_H}r}$), and because the exact density of a N -electron system exponentially decays as⁵⁴ $n(r) \rightarrow e^{-2\sqrt{-2I^P}r}$, the orbital tuning performed via minimization of equation 7 yields an asymptotic behavior of the density close to the exact-density case.

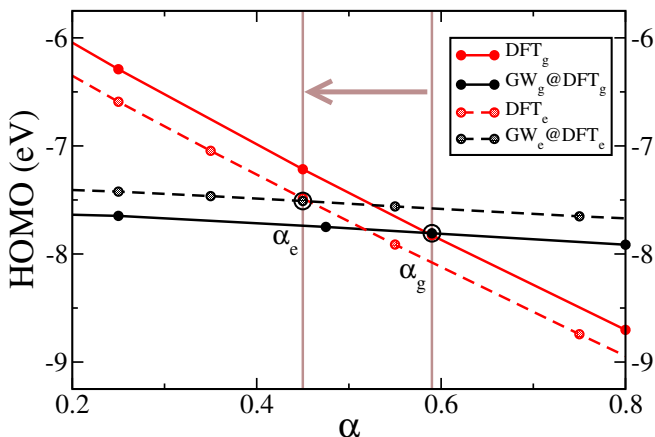
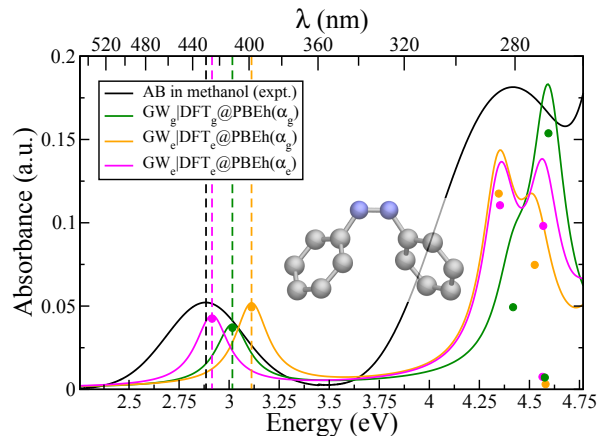


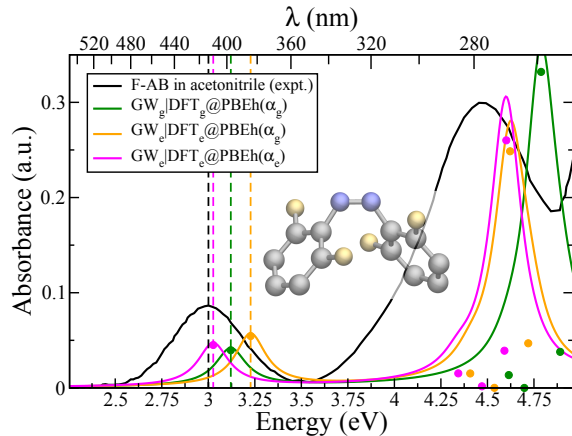
Figure 3. HOMO energy of **AB-cis** in gas and methanol-solvated phase as a function of α showing the values of α that minimize $J(\alpha)$ for gas phase and embedding. The decrease in IP due to environmental screening effects reduces α from 0.59 to 0.45.

In Fig. 3, we show ϵ_H^{KS} and ϵ_H^{GW} computed as a function of α for gas phase **AB-cis** and see that the condition that minimizes $J(\alpha)$ is satisfied for $\alpha_g = 0.59$, where 'g' subscript, we remind, stands for gas phase. We compare the S_1 and S_2 excitation energies and oscillator strengths of *cis* and *trans* **AB** computed with this approach with recent coupled cluster calculations²⁷ performed with aug-cc-pVTZ basis set, and find an excellent agreement with our BSE/ GW_g /DFT $_g$ results. The comparison of the excitation energies is reported in Table S5, together with results from previous CASPT2⁵⁵ and recent TDDFT¹³ calculations.

The inclusion of solvent polarization at GW_e level narrows the electronic gap of *cis* and *trans* **AB** (see Fig. S5): the electron removal energies decrease as shown in Fig. 3 whereas the electron addition energies increase due to the dielectric screening of the hole and electron. This polarization effect results in a smaller value of α arising from the matching of ϵ^{GW_e} and ϵ^{KS,DFT_e} , i.e. $\alpha_e=0.45$. This lower-



(a) *1-cis*



(b) *2-cis*

Figure 4. BSE optical spectra of *1-cis* and *2-cis* calculated with different embedding schemes. For both molecules, a good agreement with experiment is obtained when the starting XCF is chosen using the environment consistent approach described in the text. Experimental spectra in acetonitrile are in black^{8,12} and are arbitrarily scaled for better comparison.

ing of α is thus needed within DFT to follow the decrease in IP and thus mimics the screening of the charged excitation by the environment. We note here that the inclusion of the ground state polarization using the SMD model, i.e. DFT $_e$, lowers the KS eigenvalues by 0.3 eV and the quasiparticle energies GW_g /DFT $_e$ by the same amount (i.e. without embedding at GW). Thus, the dynamical screening by the solvent needs to be accounted for at the GW_e level so as to determine an environment consistent IP. There has been much effort in the past few years in combining optimal tuning of range-separated hybrid functionals (OT-RSH) with classical solvation models.^{56–60} In this respect, our method bears some resemblance with the optimally tuned screened range separated hybrid functionals (OT-SRSH) approach⁶¹ coupled with a non-equilibrium PCM model, where the tuning of the amount of long-range Fock exchange is performed by using energies calculated with DFT+PCM.^{58–60,62}

We then extend this approach to compute BSE spectra of molecules in solution using the full embedding QM/MM scheme, i.e. BSE/ GW_e /DFT $_e$ @PBEh(α_e). In order to demonstrate the validity of the method, we compute the optical absorption spectra of 10 **AB** derivatives shown in Fig. 5 that exhibit varying values of S_1 band separation, $\Delta E(S_1)$, between *trans* and *cis*. For this purpose, we have chosen azo derivatives that exhibit (experimental) values of

$\Delta E(S_1)$ ranging from 0.13 eV for **1** to 0.54 eV for **6** (see Table S7 and references within). All experimental values are taken from the absorption spectra as the maxima of the $n \rightarrow \pi^*$ transition^{5,63–66} and they are tabulated in Table S7. To describe each isomer in solution we use the following procedure: (1) optimize the geometry using $\text{DFT}_e@PBE0$; (2) determine the α that minimized $J(\alpha)$, which requires few $\text{GW}_e/\text{DFT}_e@PBEh$ calculations at different α , (3) compute the optical spectra using BSE at the optimal α (see fig. 1).

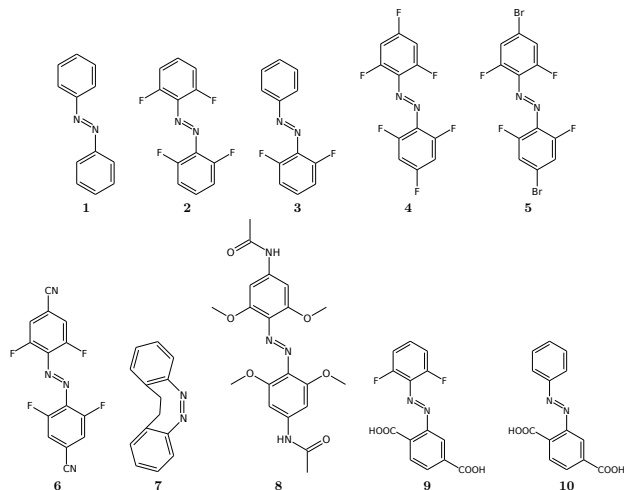


Figure 5. Schematic illustration of the **AB** derivatives studied in this work.

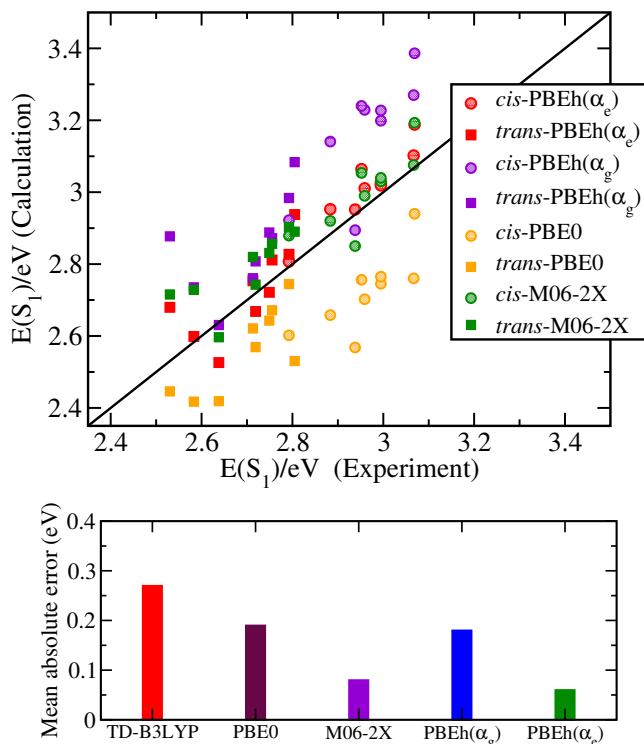


Figure 6. Experiment versus calculation comparison for the first excitation energy, $E(S_1)$, of the **AB** derivatives in the solvated phase and MAEs. The experimental values^{5,63–66} taken as reference are tabulated in Table S2. The full list of $E(S_1)$ is reported in Table S8. The MAE of TDDFT is taken from published data.⁶³

For clarity, we report first the case of **1-cis** and **2-cis**, i.e. bare **AB** and *ortho*-fluoro-**AB** (see Fig. 5). In Fig. 4 we compare the BSE spectra computed using different levels of embedding with the experimental spectra measured in ace-

tonitrile. Only a full embedding approach with the environment consistent IP choice (i.e. using α_e) reproduces the optical spectra of **1-cis** and **2-cis** molecules (magenta curves) in acetonitrile with an accuracy of less than a tenth of eV for $E(S_1)$ (see Fig. 4), compared with experiment (black curves). Similar results are found for *trans* and are reported in Figs. S6 and S7. It is interesting to note that although one would expect to improve the agreement with experiment upon inclusion of embedding with GW_e/DFT_e but using α_g (yellow curve in Fig. 4), the comparison instead worsens compared with the gas phase calculations (green curves). As for the case of acrolein, when keeping the same starting XCF, we observe a blueshift for the $n \rightarrow \pi^*$ excitation upon solvation.⁴¹ While for acrolein the blueshift resulted mainly from the effect of embedding at the DFT ground state level (Table S4), here embedding at DFT_e and GW_e contribute by similar amounts to the total shift as shown in Figs. S6 and S7. The wavefunction is also modified when the SMD model is used in DFT almost as much as upon changing α , as illustrated in Figs. S10 and S11. To further assess the accuracy of this approach we report the value of $\Delta E(S_1)$ for molecules **1** and **2** using 4 different computational schemes that gradually include the solvent effects to a full embedding scheme, and again, compare it with experiment. The S_1 excitation energies reported in Table 1 show that the best agreement with experiment is obtained with $\text{BSE}/\text{GW}_e/\text{DFT}_e@PBEh(\alpha_e)$.

Table 1. S_1 excitation energies and band separation, $\Delta E(S_1)$, in eV, of **1-trans** and *cis* and **2** computed using different embedding schemes. For clarity we use the notation $\text{DFT}(\alpha)$ rather than $\text{DFT}@PBEh(\alpha)$.

isomer			BSE/GW_g		BSE/GW_e		Exp.
	α_g	α_e	$\text{DFT}_g(\alpha_g)$	$\text{DFT}_e(\alpha_g)$	$\text{DFT}_g(\alpha_g)$	$\text{DFT}_e(\alpha_e)$	
1-trans	0.63	0.48	2.835	2.896	3.002	2.893	2.804
1-cis	0.59	0.45	3.016	3.077	3.112	2.914	2.882
1-$\Delta E(S_1)$	-	-	0.182	0.181	0.110	0.022	0.078
2-trans	0.62	0.44	2.529	2.707	2.816	2.668	2.719
2-cis	0.59	0.46	3.121	3.194	3.227	3.027	2.995
2-$\Delta E(S_1)$	-	-	0.592	0.486	0.411	0.358	0.276

Finally, the $\text{BSE}/\text{GW}_e/\text{DFT}_e@PBEh(\alpha_e)$ excitation energies of the 20 geometries (two isomers for each of the 10 derivatives) in different organic solvents are reported in Fig. 6 and compared with experimental values. It should be noted that the values of α_e are determined for each **AB** derivative and *trans-cis* configurations, and vary only slightly from case to case (from 0.35 for **5-trans** to 0.46 for **3-cis**, see Table S2 for the full list of values). An excellent agreement with experimentally observed first excitation energies is achieved for both *trans* and *cis* (see Fig. 6) with a mean absolute error (MAE) for S_1 as low as 0.06 eV. For comparison, we also compute the BSE spectra using the full embedding scheme while using i) PBE0, ii) M06-2X, and iii) $\text{PBEh}(\alpha_g)$ throughout. Thus, the calculations follow the scheme $\text{BSE}/\text{GW}_e/\text{DFT}_e@PBE0$, $\text{BSE}/\text{GW}_e/\text{DFT}_e@M06-2X$ and $\text{BSE}/\text{GW}_e/\text{DFT}_e@PBEh(\alpha_g)$, respectively. We also include results from a previous study using TDDFT@B3LYP with molecules embedded in a continuum using PCM.⁶³ All data points are shown in Fig. 6 together with the MAEs of each set of calculations. The whole set of $E(S_1)$ excitation energies are tabulated in Table S8. The MAE is slightly larger for M06-2X (0.08 eV) while it increases by more than a factor of three for PBE0 (0.19 eV). Interestingly, $\text{PBEh}(\alpha_g)$ performs similarly to PBE0 with a MAE of 0.18: while the former overestimates $E(S_1)$ in general, the latter underestimates it. This reveals again the importance of the good

amount of exact exchange. Finally, our approach largely outperforms recent embedded TDDFT calculations⁶³ with MAE=0.28 eV (data shown in Fig. S12).

In conclusion, our calculations using the Bethe-Salpeter formalism combined with a non-equilibrium embedding scheme show an excellent agreement with experiments for the lowest singlet energy of a large set of solvated azobenzene derivatives. We evidence in particular the importance of tuning the starting point functional in systems where not only the energy levels, but also the shape of the KS molecular orbitals, may vary significantly as a function of the selected functional. This may lead to significant effects in the case of the very standard non-self-consistent or partially self-consistent BSE/GW schemes where the input Kohn-Sham eigenstates are kept frozen. The alignment of the KS and GW HOMO level energies offers a mean to select the starting functional on an ab initio basis, yielding an improved asymptotic density and leading, in the present case, to an excellent agreement with experimental data.

Acknowledgement This work was funded by the French National Agency for Research (ANR-15-CE06-0003-01). Calculations were performed using resources granted by GENCI under the CINES grant number A0020907211. The froggy platform of the CIMENT infrastructure was also employed for the calculations.

Supporting Information Available: Convergence studies; BSE of acrolein in water; excitation energies and oscillator strengths of *1-trans/cis* computed with different ab initio methods; KS wavefunctions; BSE with different embedding schemes; tabulated S₁ energies and α_e ; MEAs. This material is available free of charge via the Internet at <http://pubs.acs.org/>.

Notes and References

- (1) Velema, W. A.; Van Der Berg, J. P.; Hansen, M. J.; Szymanski, W.; Driessen, A. J.; Feringa, B. L. Optical control of antibacterial activity. *Nature chemistry* **2013**, *5*, 924.
- (2) Beharry, A. A.; Sadvoski, O.; Woolley, G. A. Azobenzene photoswitching without ultraviolet light. *J. Am. Chem. Soc.* **2011**, *133*, 19684–19687.
- (3) Matsunaga, D.; Asanuma, H.; Komiyama, M. Photoregulation of RNA digestion by RNase H with Azobenzene-tethered DNA. *J. Am. Chem. Soc.* **2004**, *126*, 11452–11453.
- (4) Wang, F.; Liu, X.; Willner, I. DNA Switches: from Principles to Applications. *Angew. Chem. Int. Ed.* **2015**, *54*, 1098–1129.
- (5) Park, J.; Yuan, D.; Pham, K. T.; Li, J.-R.; Yakovenko, A.; Zhou, H.-C. Reversible alteration of CO₂ adsorption upon photochemical or thermal treatment in a metal–organic framework. *J. Am. Chem. Soc.* **2011**, *134*, 99–102.
- (6) Yang, C.-T.; Kshirsagar, A. R.; Eddin, A. C.; Lin, L.-C.; Poloni, R. Tuning Gas Adsorption by Metal Node Blocking in Photoresponsive Metal–Organic Frameworks. *Chem. Eur. J.* **2018**, *24*, 15167–15172.
- (7) Wang, Z.; Knebel, A.; Grosjean, S.; Wagner, D.; Bräse, S.; Wöll, C.; Caro, J.; Heinke, L. Tunable Molecular Separation by Nanoporous Membranes. *Nat. Commun.* **2016**, *7*, 13872.
- (8) Vetráková, L.; Ladányi, V.; Al Anshori, J.; Dvořák, P.; Wirz, J.; Heger, D. The absorption spectrum of cis-azobenzene. *Photochem. Photobiol. Sci.* **2017**, *16*, 1749–1756.
- (9) Zimmerman, G.; Chow, L.-Y.; Paik, U.-J. The Photochemical Isomerization of Azobenzene. *J. Am. Chem. Soc.* **1958**, *80*, 3528–3531.
- (10) Bandara, H. M. D.; Burdette, S. C. Photoisomerization in Different Classes of Azobenzene. *Chem. Soc. Rev.* **2012**, *41*, 1809–1825.
- (11) Siewertsen, R.; Neumann, H.; Buchheim-Stehn, B.; Herges, R.; Näther, C.; Renth, F.; Temps, F. Highly Efficient Reversible Z-E Photoisomerization of a Bridged Azobenzene with Visible Light through Resolved S₁ ($\pi\pi^*$) Absorption Bands. *J. Am. Chem. Soc.* **2009**, *131*, 15594–15595.
- (12) Bleger, D.; Schwarz, J.; Brouwer, A. M.; Hecht, S. o-Fluoroazobenzenes as readily synthesized photoswitches offering nearly quantitative two-way isomerization with visible light. *J. Am. Chem. Soc.* **2012**, *134*, 20597–20600.
- (13) Pal, A. K.; Duignan, T. J.; Autschbach, J. Calculation of Linear and Nonlinear Optical Properties of Azobenzene Derivatives with Kohn–Sham and Coupled-Cluster Methods. *Phys. Chem. Chem. Phys.* **2018**, *20*, 7303–7316.

- (14) Perdew, J. P.; Levy, M. Comment on “Significance of the Highest Occupied Kohn-Sham Eigenvalue”. *Phys. Rev. B* **1997**, *56*, 16021–16028.
- (15) Perdew, J. P.; Parr, R. G.; Levy, M.; Balduz, J. L. Density-Functional Theory for Fractional Particle Number: Derivative Discontinuities of the Energy. *Phys. Rev. Lett.* **1982**, *49*, 1691–1694.
- (16) Almladh, C. O.; Pedroza, A. C. Density-Functional Exchange-Correlation Potentials and Orbital Eigenvalues for light atoms. *Phys. Rev. A* **1984**, *29*, 2322–2330.
- (17) Casida, M. E. Correlated Optimized Effective-Potential Treatment of the Derivative Discontinuity and of the Highest Occupied Kohn-Sham Eigenvalue: A Janak-type Theorem for the Optimized Effective-Potential Model. *Phys. Rev. B* **1999**, *59*, 4694–4698.
- (18) Chong, D. P.; Gritsenko, O. V.; Baerends, E. J. Interpretation of the Kohn-Sham Orbital Energies as Approximate Vertical Ionization Potentials. *J. Chem. Phys.* **2002**, *116*, 1760–1772.
- (19) Strinati, G. Application of the Green’s Functions Methods to the Study of the Optical Properties of Semiconductors. *Riv. Nuovo Cim.* **1988**, *11*, 1–86.
- (20) Onida, G.; Reining, L.; Rubio, A. Electronic Excitations: Density-Functional versus Many-Body Green’s-Function Approaches. *Rev. Mod. Phys.* **2002**, *74*, 601–659.
- (21) Sottile, F.; Marsili, M.; Olevano, V.; Reining, L. Efficient Ab Initio Calculations of Bound and Continuum Excitons in the Absorption Spectra of Semiconductors and Insulators. *Phys. Rev. B* **2007**, *76*, 161103.
- (22) Jacquemin, D.; Duchemin, I.; Blase, X. Is the Bethe-Salpeter formalism accurate for excitation energies? Comparisons with TD-DFT, CASPT2, and EOM-CCSD. *J. Phys. Chem. Lett.* **2017**, *8*, 1524–1529.
- (23) Bruneval, F.; Hamed, S. M.; Neaton, J. B. A Systematic Benchmark of the Ab Initio Bethe-Salpeter Equation Approach for Low-lying Optical Excitations of Small Organic Molecules. *J. Chem. Phys.* **2015**, *142*, 244101.
- (24) Jacquemin, D.; Duchemin, I.; Blase, X. Benchmarking the Bethe-Salpeter Formalism on a Standard Organic Molecular Set. *J. Chem. Theory Comput.* **2015**, *11*, 3290–3304.
- (25) Cembran, A.; Bernardi, F.; Garavelli, M.; Gagliardi, L.; Orlandi, G. On the Mechanism of the cis-trans Isomerization in the Lowest Electronic States of Azobenzene: S₀, S₁, and T₁. *J. Am. Chem. Soc.* **2004**, *126*, 3234–3243.
- (26) Conti, I.; Garavelli, M.; Orlandi, G. The Different Photoisomerization Efficiency of Azobenzene in the Lowest $\pi\pi^*$ and $\pi\pi^*$ Singlets: The Role of a Phantom State. *J. Am. Chem. Soc.* **2008**, *130*, 5216–5230.
- (27) Fliegl, H.; Köhn, A.; Hättig, C.; Ahlrichs, R. Ab Initio Calculation of the Vibrational and Electronic Spectra of trans- and cis-Azobenzene. *J. Am. Chem. Soc.* **2003**, *125*, 9821–9827.
- (28) Baumeier, B.; Andrienko, D.; Rohlfing, M. Frenkel and Charge-Transfer Excitations in Donor-acceptor Complexes from Many-Body Green’s Functions Theory. *J. Chem. Theory Comput.* **2012**, *8*, 2790–2795.
- (29) Faber, C.; Boulanger, P.; Attaccalite, C.; Duchemin, I.; Blase, X. Excited states properties of organic molecules: from density functional theory to the GW and Bethe-Salpeter Green’s function formalisms. *Phil. Trans. R. Soc. A* **2014**, *372*, 20130271.
- (30) Baumeier, B.; Rohlfing, M.; Andrienko, D. Electronic Excitations in Push-Pull Oligomers and Their Complexes with Fullerene from Many-Body Green’s Functions Theory with Polarizable Embedding. *J. Chem. Theory Comput.* **2014**, *10*, 3104–3110.
- (31) Li, J.; D’Avino, G.; Duchemin, I.; Beljonne, D.; Blase, X. Combining the Many-Body GW Formalism with Classical Polarizable Models: Insights on the Electronic Structure of Molecular Solids. *J. Phys. Chem. Lett.* **2016**, *7*, 2814–2820.
- (32) Duchemin, I.; Jacquemin, D.; Blase, X. Combining the GW formalism with the polarizable continuum model: A state-specific non-equilibrium approach. *J. Chem. Phys.* **2016**, *144*, 164106.
- (33) Wehner, J.; Brombacher, L.; Brown, J.; Junghans, C.; Çaylak, O.; Khalak, Y.; Madhikar, P.; Tirimbò, G.; Baumeier, B. Electronic Excitations in Complex Molecular Environments: Many-Body Green’s Functions Theory in VOTCA-XTP. *J. Chem. Theory Comput.* **2018**, *14*, 6253–6268.
- (34) Blase, X.; Attaccalite, C. Charge-Transfer Excitations in Molecular Donor-Acceptor Complexes within the Many-Body Bethe-Salpeter Approach. *Appl. Phys. Lett.* **2011**, *99*, 171909.
- (35) Blase, X.; Attaccalite, C.; Olevano, V. First-Principles GW calculations for fullerenes, porphyrins, phthalocyanine, and other molecules of interest for Organic Photovoltaic Applications. *Phys. Rev. B* **2011**, *83*, 115103.
- (36) Valiev, M.; Bylaska, E.; Govind, N.; Kowalski, K.; Straatsma, T.; Dam, H. V.; Wang, D.; Nieplocha, J.; Apra, E.; Windus, T.; de Jong, W. NWChem: A Comprehensive and Scalable Open-Source Solution for Large Scale Molecular Simulations. *Comput. Phys. Commun.* **2010**, *181*, 1477–1489.
- (37) Kaplan, F.; Harding, M. E.; Seiler, C.; Weigend, F.; Evers, F.; van Setten, M. J. Quasi-Particle Self-Consistent GW for Molecules. *J. Chem. Theory Comput.* **2016**, *12*, 2528–2541.
- (38) Marenich, A. V.; Cramer, C. J.; Truhlar, D. G. Universal Solvation Model based on Solute Electron Density and on a Continuum Model of the Solvent defined by the Bulk Dielectric Con-

- stant and Atomic Surface Tensions. *J. Phys. Chem. B* **2009**, *113*, 6378–6396.
- (39) Winget, P.; Dolney, D. M.; Giesen, D. J.; Cramer, C. J.; Truhlar, D. G. Minnesota solvent descriptor database. *Dept. of Chemistry and Supercomputer Inst., University of Minnesota, Minneapolis, MN* **1999**, 55455.
- (40) Li, J.; D’Avino, G.; Duchemin, I.; Beljonne, D.; Blase, X. Accurate description of charged excitations in molecular solids from embedded many-body perturbation theory. *Phys. Rev. B* **2018**, *97*, 035108.
- (41) Duchemin, I.; Guido, C. A.; Jacquemin, D.; Blase, X. The Bethe–Salpeter formalism with polarisable continuum embedding: reconciling linear-response and state-specific features. *Chem. Sci.* **2018**, *9*, 4430–4443.
- (42) D’Avino, G.; Muccioli, L.; Zannoni, C.; Beljonne, D.; Soos, Z. G. Electronic Polarization in Organic Crystals: A Comparative Study of Induced Dipoles and Intramolecular Charge Redistribution Schemes. *J. Chem. Theory Comput.* **2014**, *10*, 4959–4971.
- (43) The same database is used within NWchem to implement the SMD model, see <http://comp.chem.umn.edu/solvation/mnsddb.pdf>.
- (44) Adamo, C.; Barone, V. Toward reliable density functional methods without adjustable parameters: The PBE0 model. *J. Chem. Phys.* **1999**, *110*, 6158–6170.
- (45) Dunning Jr, T. H. Gaussian Basis Sets for Use in Correlated Molecular Calculations. I. The Atoms Boron through Neon and Hydrogen. *J. Chem. Phys.* **1989**, *90*, 1007–1023.
- (46) Woon, D. E.; Dunning Jr, T. H. Gaussian basis sets for use in correlated molecular calculations. III. The atoms aluminum through argon. *J. Chem. Phys.* **1993**, *98*, 1358–1371.
- (47) Burke, K.; Ernzerhof, M.; Perdew, J. P. The Adiabatic Connection Method: a Non-empirical Hybrid. *Chemical Physics Letters* **1997**, *265*, 115–120.
- (48) Perdew, J. P.; Burke, K.; Ernzerhof, M. Generalized Gradient Approximation Made Simple. *Phys. Rev. Lett.* **1996**, *77*, 3865–3868.
- (49) Blase, X.; Duchemin, I.; Jacquemin, D. The Bethe–Salpeter Equation in Chemistry: Relations with TD–DFT, Applications and Challenges. *Chem. Soc. Rev.* **2018**, *47*, 1022–1043.
- (50) Zhao, Y.; Truhlar, D. G. The M06 Suite of Density Functionals for Main Group Thermochemistry, Thermochemical Kinetics, Noncovalent Interactions, Excited States, and Transition Elements: Two New Functionals and Systematic Testing of Four M06-class Functionals and 12 other Functionals. *Theor. Chem. Acc.* **2008**, *120*, 215–241.
- (51) Levy, M.; Perdew, J. P.; Sahni, V. Exact differential equation for the density and ionization energy of a many-particle system. *Phys. Rev. A* **1984**, *30*, 2745.
- (52) Perdew, J. P.; Parr, R. G.; Levy, M.; Balduz Jr, J. L. Density-functional theory for fractional particle number: derivative discontinuities of the energy. *Phys. Rev. Lett.* **1982**, *49*, 1691.
- (53) Perdew, J. P.; Levy, M. Comment on “Significance of the highest occupied Kohn–Sham eigenvalue”. *Phys. Rev. B* **1997**, *56*, 16021.
- (54) Katriel, J.; Davidson, E. R. Asymptotic behavior of atomic and molecular wave functions. *Proc. Natl. Acad. Sci.* **1980**, *77*, 4403–4406.
- (55) Conti, I.; Garavelli, M.; Orlandi, G. The different photoisomerization efficiency of azobenzene in the lowest $n\pi^*$ and $\pi\pi^*$ singlets: the role of a phantom state. *J. Am. Chem. Soc.* **2008**, *130*, 5216–5230.
- (56) Sachse, T.; Martínez, T. J.; Presselt, M. On combining the conductor-like screening model and optimally tuned range-separated hybrid density functionals. *J. Chem. Phys.* **2019**, *150*, 174117.
- (57) Kronik, L.; Kümmel, S. Dielectric screening meets optimally tuned density functionals. *Adv. Mater.* **2018**, *30*, 1706560.
- (58) Bhandari, S.; Dunietz, B. D. Quantitative Accuracy in Calculating Charge Transfer State Energies in Solvated Molecular Complexes Using a Screened Range Separated Hybrid Functional within a Polarized Continuum Model. *J. Chem. Theory Comput.* **2019**, *15*, 4305–4311.
- (59) Zheng, Z.; Egger, D. A.; Bredas, J.-L.; Kronik, L.; Coropceanu, V. Effect of solid-state polarization on charge-transfer excitations and transport levels at organic interfaces from a screened range-separated hybrid functional. *J. Phys. Chem. Lett.* **2017**, *8*, 3277–3283.
- (60) Bhandari, S.; Cheung, M. S.; Geva, E.; Kronik, L.; Dunietz, B. D. Fundamental Gaps of Condensed-Phase Organic Semiconductors from Single-Molecule Calculations using Polarization-Consistent Optimally Tuned Screened Range-Separated Hybrid Functionals. *J. Chem. Theory Comput.* **2018**, *14*, 6287–6294.
- (61) Refaely-Abramson, S.; Sharifzadeh, S.; Jain, M.; Baer, R.; Neaton, J. B.; Kronik, L. Gap renormalization of molecular crystals from density-functional theory. *Phys. Rev. B* **2013**, *88*, 081204.
- (62) Joo, B.; Han, H.; Kim, E.-G. Solvation-mediated tuning of the range-separated hybrid functional: Self-sufficiency through screened exchange. *J. Chem. Theory Comput.* **2018**, *14*, 2823–2828.
- (63) Knie, C.; Utecht, M.; Zhao, F.; Kulla, H.; Kovalenko, S.; Brouwer, A. M.; Saalfrank, P.; Hecht, S.; Bleger, D. ortho-Fluoroazobenzenes: Visible Light Switches with Very Long-Lived Z Isomers. *Chem. Eur. J.* **2014**, *20*, 16492–16501.
- (64) Siewertsen, R.; Schönborn, J. B.; Hartke, B.; Renth, F.; Temps, F. Superior Z→E and E→Z Photoswitching Dynamics of dihydrodibenzodiazocine, a Bridged Azobenzene, by S_1 ($n-\pi^*$) Excitation at $\lambda = 387$ and 490 nm. *Phys. Chem. Chem. Phys.* **2011**, *13*, 1054–1063.
- (65) Beharry, A. A.; Sadovski, O.; Woolley, G. A. Azobenzene Photo-switching without Ultraviolet Light. *J. Am. Chem. Soc.* **2011**, *133*, 19684–19687.
- (66) Müller, K.; Knebel, A.; Zhao, F.; Bléger, D.; Caro, J.; Heinke, L. Switching Thin Films of Azobenzene-Containing Metal–Organic Frameworks with Visible Light. *Chem. Eur. J.* **2017**, *23*, 5434–5438.

Graphical TOC Entry

